Supplementary data for

Enhancing the interfacial carrier dynamic in perovskite solar cells with ultra-thin single-crystalline nanograss-like TiO_2 electron transport layer

Akrajas Ali Umar[1,3#]*, Xin Zhang[#2], Siti Khatijah Md Saad[1], Nurul Ain Abd Malek[1], Kai Liu[3], Nabilah Alias[1], Nur Adliha Abdullah[1], Xiaoguo Li[3], Fengcai Liu[3], Zejiao Shi[3], Haijuan Zhang[3], Chongyuan Li[3], Zhenhua Weng[3], Yiting Liu[4], Yuyi Zhang[4], Xiaolei Zhang[4], Jiao Wang[3], Yiqiang Zhan[2,3]*

[1]Institute of Microengineering and Nanoelectronics, Universiti Kebangsaan Malaysia, 43600 UKM Bangi, Selangor, Malaysia.

[2]Academy for Engineering & Technology, Fudan University, Shanghai 200433, China.

[3]Center for Micro Nano Systems, School of Information Science and Technology (SIST), Fudan University, Shanghai 200433, China.

[4]State Key Laboratory of Precision Spectroscopy, East China Normal University, Shanghai 200062, China.

*Corresponding author: AAU (akrajas@ukm.edu.my), YZ (yqzhan@fudan.edu.cn).

[#]These authors contribute equally to this work.

Table S1. Photovoltaic parameters of PSC using TNG with different length at perovskite concentration of 1.3 M and using optimum TNG (TNG50) at different perovskite concentration.

Sample	Length (nm)	J_{sc} (mA cm^{-2}) ***@maxPCE**.(avg.)*	V_{oc} (Volt) ***@maxPCE**.(avg.)*	*FF* (%) ***@maxPCE.**(avg.)*	*PCE* (%) ***@maxPCE**.(avg.)*	*HI*	J_{EQE} (mA cm^{-2})
PSC using TNG with different length at perovskite concentration of 1.3 M							
SnO2	-	**21.31**(21.02 ± 0.52)	**1.15**(1.13 ± 0.01)	**0.743**(0.743 ± 2.09)	**18.21**(17.65 ± 0.35)	0.124144	19.98
Colloidal TiO_2		**22.82**(22.54 ± 0.31)	**1.14**(1.13 ± 0.01)	**0.778**(0.775 ± 0.36)	**20.23**(19.74 ± 0.47)	-	-
TNG25	40	**22.55**(21.56 ± 0.36)	**1.17**(1.16 ± 0.01)	**0.796**(0.799 ± 0.40)	**21.00**(19.98 ± 0.50)	0.052295	20.49
TNG50	80	**23.30**(22.82 ± 0.43)	**1.16**(1.15 ± 0.02)	**0.799**(0.794 ± 0.75)	**21.60**(20.84 ± 0.33)	0.101718	20.25
TNG75	120	**22.56**(21.70 ± 0.56)	**1.17**(1.17 ± 0.01)	**0.803**(0.798 ± 0.73)	**21.20**(20.26 ± 0.55)	0.040414	20.53
TNG100	250	**22.46**(21.50 ± 0.60)	**1.16**(1.16 ± 0.01)	**0.796**(0.792 ± 1.94)	**20.74**(19.75 ± 0.73)	0.068743	20.18
TNG125	200	**21.96**(21.85 ± 0.45)	**1.13**(1.11 ± 0.01)	**0.798**(0.781 ± 2.24)	**19.80**(18.94 ± 0.51)	0.055131	19.41
TNG150	200	**22.24**(21.84 ± 0.76)	**1.12**(1.09 ± 0.03)	**0.782**(0.782 ± 1.57)	**19.48**(18.62 ± 0.60)	0.099506	19.03
TNG50 based PSC using different perovskite (PVK) conc.							
PVK 1.1 M		**23.03**(22.30 ± 0.44)	**1.15**(1.14 ± 0.01)	**0.788**(0.777 ± 1.13)	**20.87**(19.75 ± 0.63)	0.110495	
PVK 1.2 M		**22.96**(22.54 ± 0.34)	**1.15**(1.15 ± 0.01)	**0.783**(0.784 ± 0.50)	**20.67**(20.32 ± 0.37)	0.123327	
PVK 1.3 M		**23.30**(22.82 ± 0.43)	**1.16**(1.15 ± 0.02)	**0.799**(0.794 ± 0.75)	**21.60**(20.84 ± 0.33)	0.101718	
PVK 1.4 M		**23.16**(23.01 ± 0.31)	**1.15**(1.12 ± 0.02)	**0.793**(0.784 ± 1.09)	**21.12**(20.20 ± 0.65)		
PVK 1.5 M		**23.96**(23.26 ± 0.42)	**1.11**(1.09 ± 0.04)	**0.776**(0.771 ± 0.10)	**20.64**(19.55 ± 0.82)		

Table S2. Fitted parameters for TRPL and EIS spectroscopy.

Sample		TNG	SnO_2
TRPL	Model	ExpDecay2	
	Equation	y = y0 + A1*exp(-x/t1) + A2*exp(-x/t2)	
	y0	-0.06383	-0.19882
	A1	10.09526	0.67254
	τ1	3.3	7.1
	A2	0.64151	1.09695
	τ2	64.8	78.5
	Reduced Chi-Sqr	5.59156E-04	7.78087E-04
	R-Square (COD)	0.97808	0.9819833
	Adj. R-Square	0.97802	0.98194
EIS	Rs (**Ω**)	11.52	11.4
	Rct (**Ω**)	111	431
	Rrec (**Ω**)	134	543

Table S3. Comparison of interfacial charge transfer dynamic on our new ETL evaluated by transient PL analysis with those on the currently reported data.

Sample	τ_1 (ns)	τ_2 (ns)	$\tau_{average}$ (ns)	PCE (%)	Perovskite	Ref.
TNG-50	3.3	64.8	-	21.6	$Cs_{0.05}[MA_{0.13}FA_{0.87}]_{0.95}Pb(I_{0.87}Br_{0.13})_3$	Current results
SnO_2	7.1	78.5	-	18.21		
TiO_2	-	-	130.67	17.46	$MAPbI_3$	[1]
PCBM/ TiO_2	-	-	28.81	18.94		
n-type doping PCBM/ TiO_2	-	-	26.97	20.14		
SnO_2	42.05	-	-	19.56	$CsFAMAPb(I_xBr_{1-x})_3$	[2]
Graphitic Carbon Nitride-SnO_2	12.7	-	-	21.24		
SnO_2	16.9	124.4	109.1	19.1	$(FAPbI_3)_{0.95}(MAPbBr_3)_{0.05}$	[3]
SnO_2-KCl	8.8	161.1	139.6	21.6		
SnO_2	-	-	39.95	19.04	$MAPbI_3$	[4]
SnO_2 /Pyrrolidinofullerene	-	-	24.98	21.39		
SnO_2	10.9	147.5	142.14	15.13	$MAPbI_3$	[5]
Nb doped SnO_2	6.18	45.49	42.71	17.57		
TiO_2 (41 nm)	4.45	154.42	87.97	18.72	$MAPbI_3$	[6]
TiO_2/ZrO_2/carbon triple-layer mesoscopic scaffold	-	-	93.79	14.39	$MAPbI_3$	[7]

Table S4. Comparison of carrier transport dynamic in our device evaluated by electrochemical impedance spectroscopy with those in the recently reported data.

Sample	R_S (Ω)	R_{CT} (Ω)	R_{REC} (Ω)	PCE (%)	Perovskite	Ref.
TNG-50	8.5	111	134	21.6	$Cs_{0.05}[MA_{0.13}FA_{0.87}]_{0.95}Pb(I_{0.87}Br_{0.13})_3$	Current results
SnO_2	11.85	431	543	18.21		
Pristine WO_3	-	68	1640	17.04	$MAPbI_3$	8
TiO_2/WO_3	-	70	2910	20.14		
SnO_2	2.25	18.81	421.25	20.06	$(FAPbI_3)_{0.85}(MAPbBr_3)_{0.15}$	9
K-doped TiO_2	1.3	7.5	425	19.8	$Cs_x(FA_{0.83}MA_{0.17})_{(1-x)}Pb(I_{0.83}Br_{0.17})_3$	10
Pristine TiO_2	6	2.1	-	18		
Crystal-TiO_2	17.5	-	-	18.65	$Cs_{0.05}[FMA_{0.15}FA_{0.85}]_{0.95}Pb(I_{0.85}Br_{0.35})_3$	11
amorphous-SnO_2	15	-	-	20.01		
Crystal -TiO_2/ amorphous -SnO_2	13	-	-	21.11		
Thermal PCBM	~20	-	271.3	18.1	$(CsPbI_3)_{0.05}(FAPbI_3)_{0.95}(MAPbBr_3)_{0.05}$	12
Laser PCBM	~20	-	639.6	20.98		
Thermal Annealing ZnO	38.5	132.6	168.8	14.34	$MAPbI_3$	13
Solvent Annealing ZnO	39.4	128.8	256.2	16.53		
TiO_2 NP	~50	~700	1668	12.17	$MAPbI_xCl_{3-x}$	14
Orchid-like TiO_2 NW	~50	~900	2795	12.97		
Ag/ Orchid-like TiO_2 NW	~50	~900	3404	14.18		
Pristine SnO_2	-	-	6.48×10^3	17.3	$MA_yFA_{1-y}Pb(I_xBr_{1-x})_3$	15
Zr doped SnO_2	-	-	9.58×10^3	19.54		
SnO_2	-	$8.3x10^3$	3.0×10^3	15.29	$MAPbI_3$	16
Li-SnO_2	-	$6.5x10^3$	6.8×10^3	18.2		
TiO_2	~4	6.2	25.9	15.71	$MAPbI_3$	17
TiO_2 /SiO_{x-10}	~4	8.02	46.3	18		
SnO_2	~17	15.9	20.65	19.04	$MAPbI_3$	4

SnO_2 /Pyrrolidinofullerene	~16	106	86.45	20.78		
TiO_2	93.4	-	1345	17.2	$MAPbI_3$	18
TiO_2 /Heaparin Sodium	81.1	-	2138	20.1		
TiO_2	~20	320	-	13.53	$MAPbI_3$	19
TiO_2-0.1 wt% SWCNT	~20	376	-	16.11		
PCBM	3.8	-	2380	19.4	$MAPbI_3$	20
C_{60}-SAM/PCBM	2.08	~570	-	19.3	$MAPbI_3$	21
PCBM	7.5	-	896	11.47	$MAPbI_3$	22

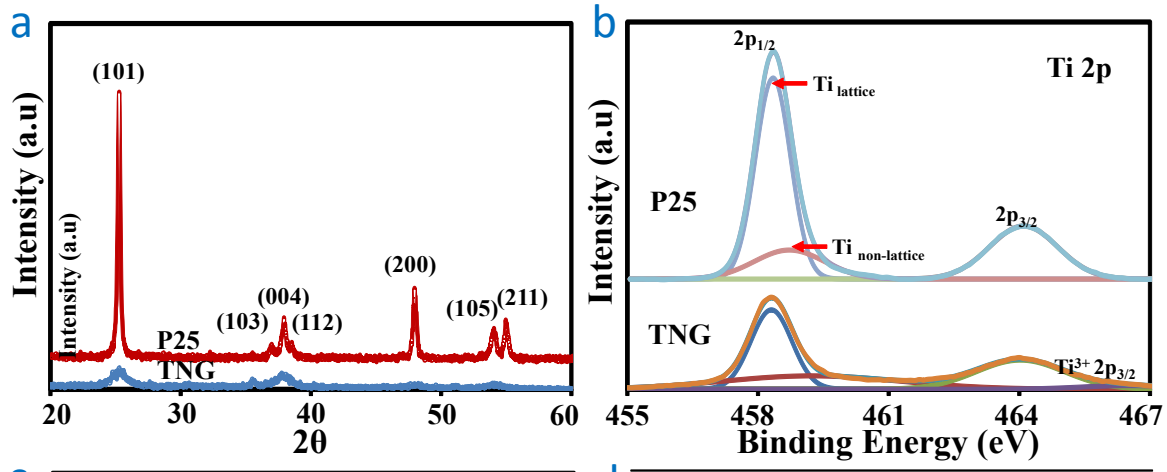

d

Peak	TNGH BE (eV)	TNGH %	P25 BE (eV)	P25 %
O_L lattice	529.44	43.08	529.57	59.10
O_B bridging	529.83	23.46	530.39	34.12
O_H hydroxyl	530.35	33.46	531.84	6.78
Ti $2p_{1/2}$ lattice	458.31	38.18	458.34	55.48
Ti $2p_{3/2}$ lattice	459.23	27.77	458.72	16.03
Ti $2p_{1/2}$ non-lattice	464.02	29.95	464.10	28.49
Ti $2p_{3/2}$ non-lattice	466.52	4.10	-	-

Figure S1. Phase crystallinity and surface chemistry properties of TiO_2 nanograss. (a) X-ray diffraction spectra of TiO_2 nanograss and P25 (for comparison). TiO_2 nanograss exhibits much high ratio of I_{004}/I_{101} compared to the P25, reflecting the TiO_2 nanograss dominated by

(001) high-energy plane. (b and c) XPS spectra for Ti 2p and O 1s. (d) detailed chemical state properties of Ti 2p and O 1s.

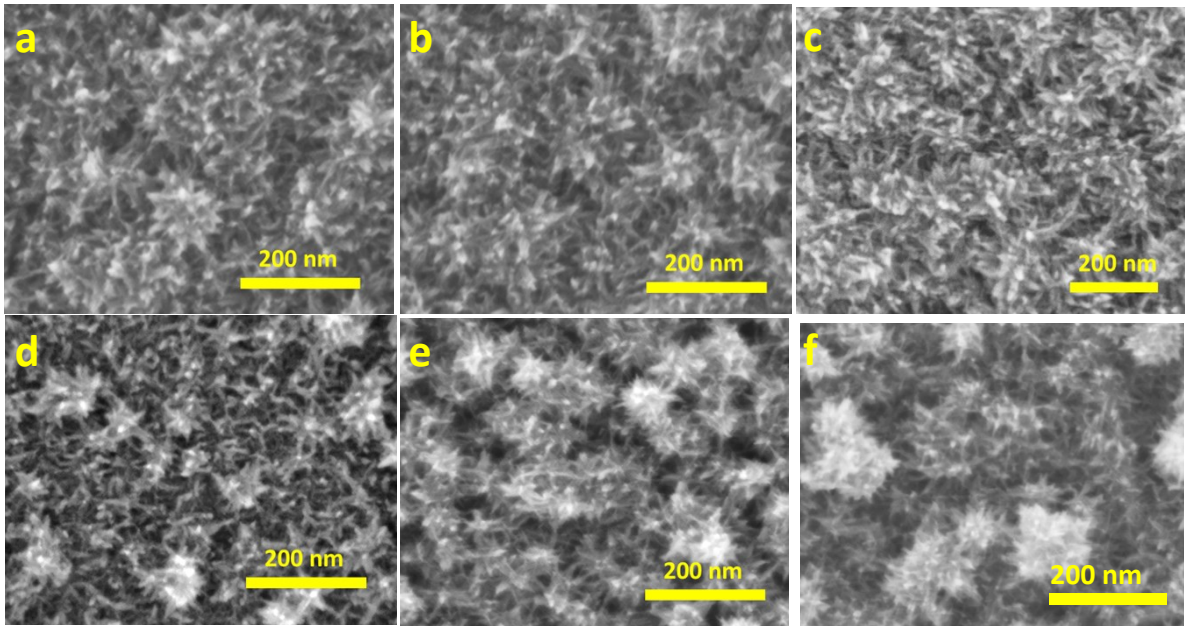

Figure S2. FESEM image of TiO_2 nanograss on ITO substrate prepared using different HMT concentration. (a) 2 mL of 0.025, (b) 2 mL of 0.05, (c) 2 mL of 0.075, (d) 2 mL of 0.1, (e) 2 mL of 0.125 and (f) 2 mL of 0.15 mM. Ammonium hexafluoro titanate and acid boric are kept at 5 mL of 0.1 M and 5 mL of 0.2 M, respectively.

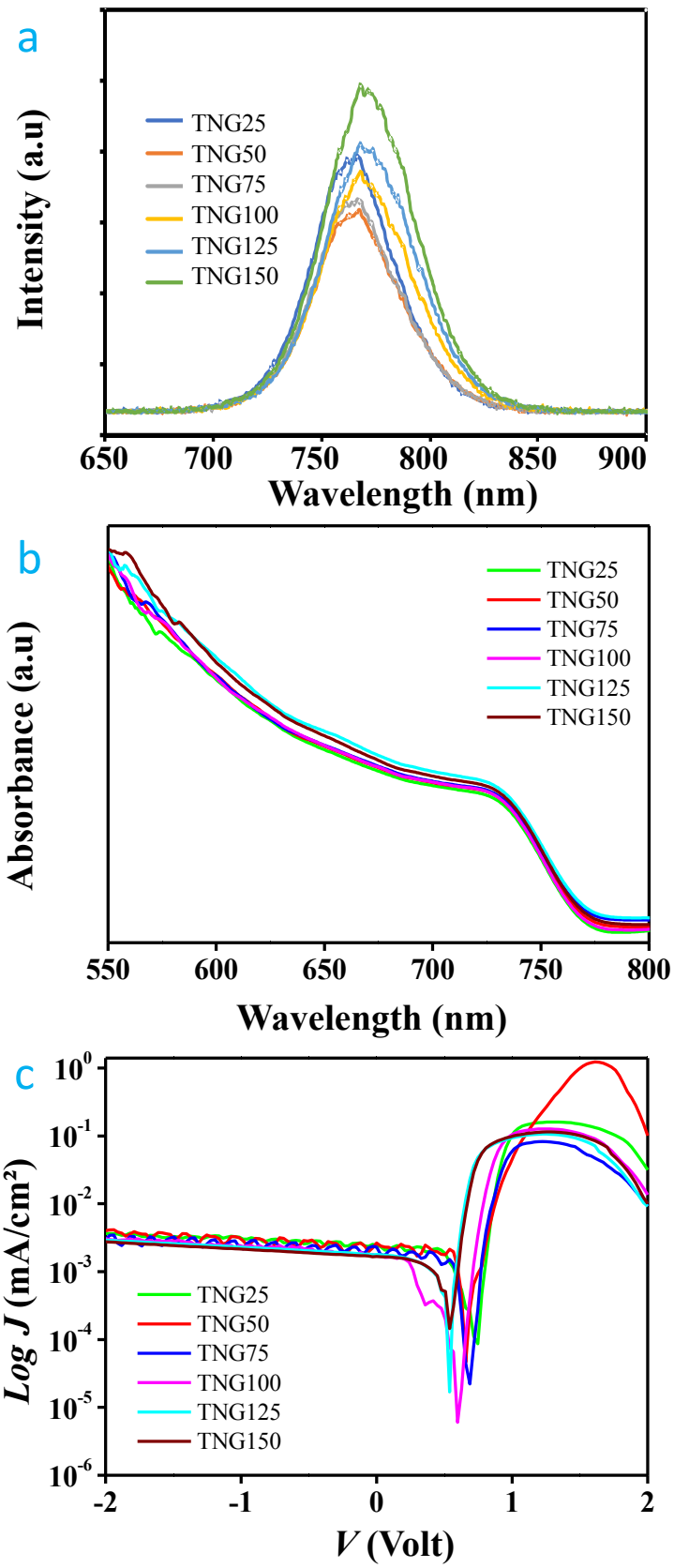

Figure S3. Optical and electrical properties of PSC device using different length of TNG. (a) photoluminescence, (b) optical absorbance and (c) J-V curve under dark.

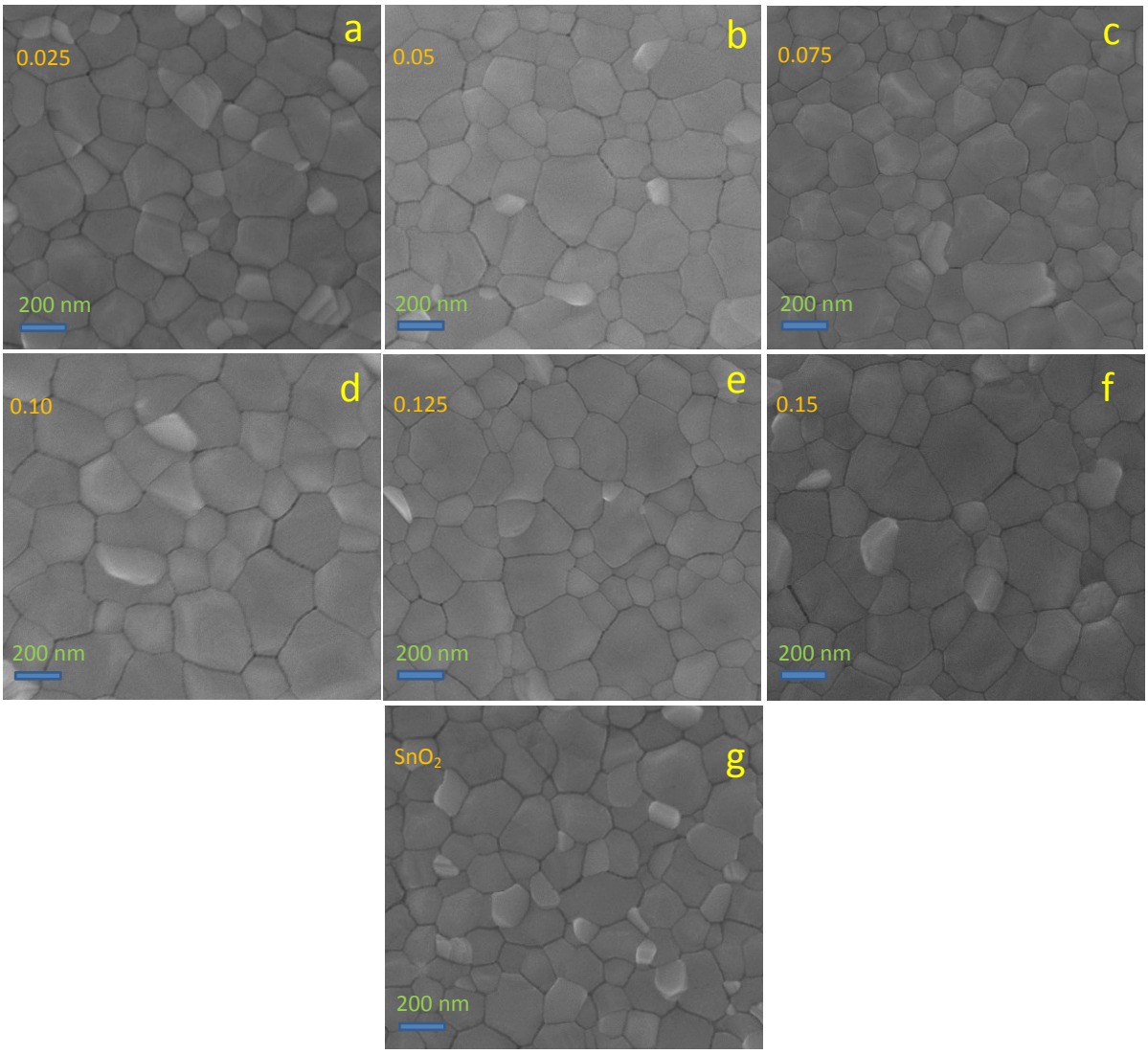

Figure S4. Perovskite film morphology on TNG with different length. a to f are FESEM of perovskite absorber layer on TNG with different length, i.e. 40 (a), 80 (b), 120 (c), 250 (d), 200 (e) and 200 nm (f). g is perovskite layer morphology on SnO_2 ETL.

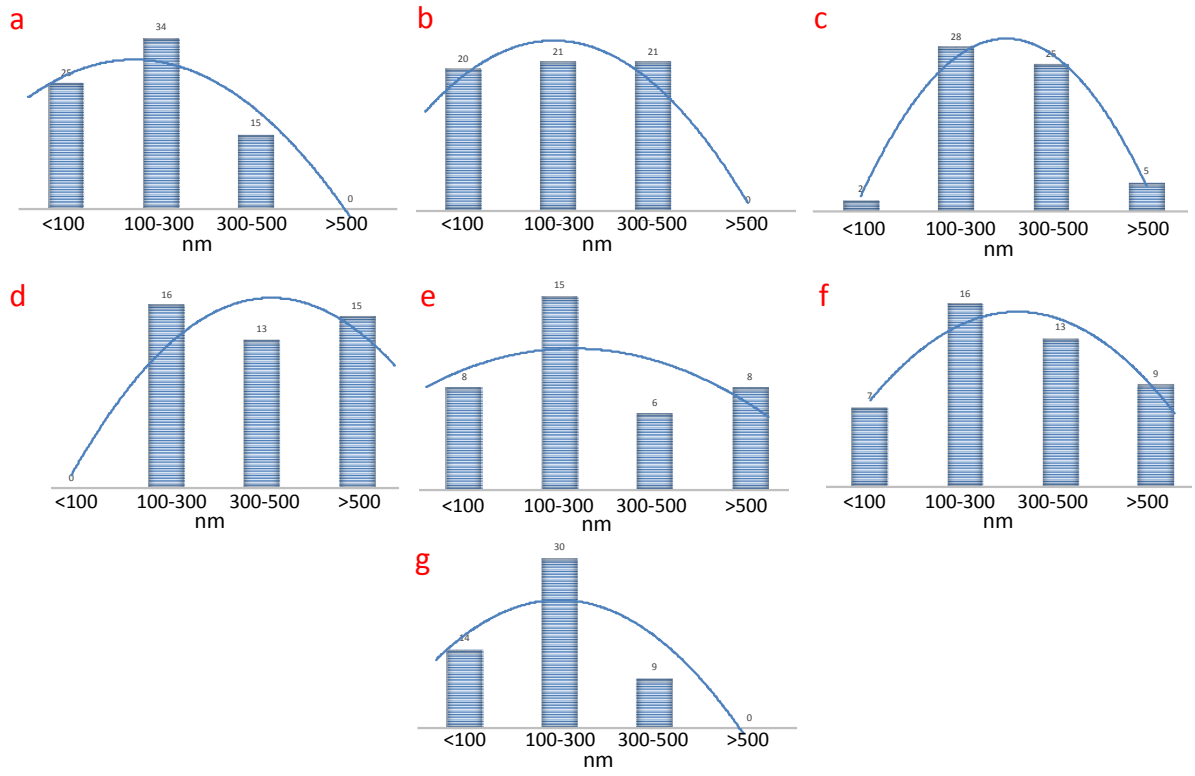

Figure S5. Perovskite grain size distribution on TNG with different length. (a) TNG25, (b) TNG50, (c) TNG75, (d) TNG100, (e) TNG125 and (f) TNG150. g is perovskite grain size distribution on SnO_2 for comparison.

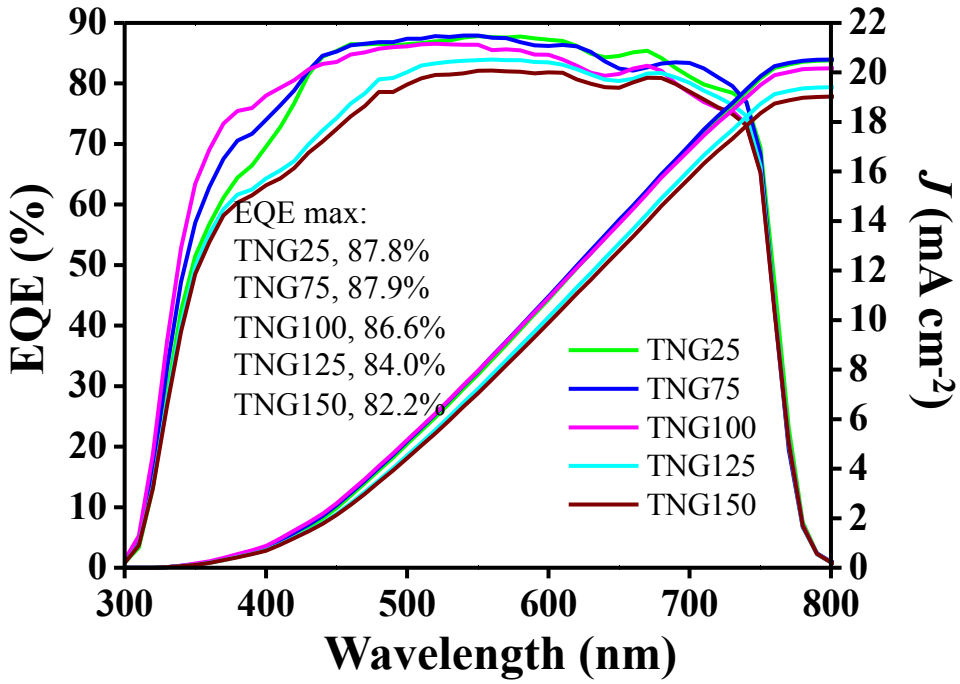

Figure S6. EQE spectra and integrated current density of PSC device using TNG with different length.

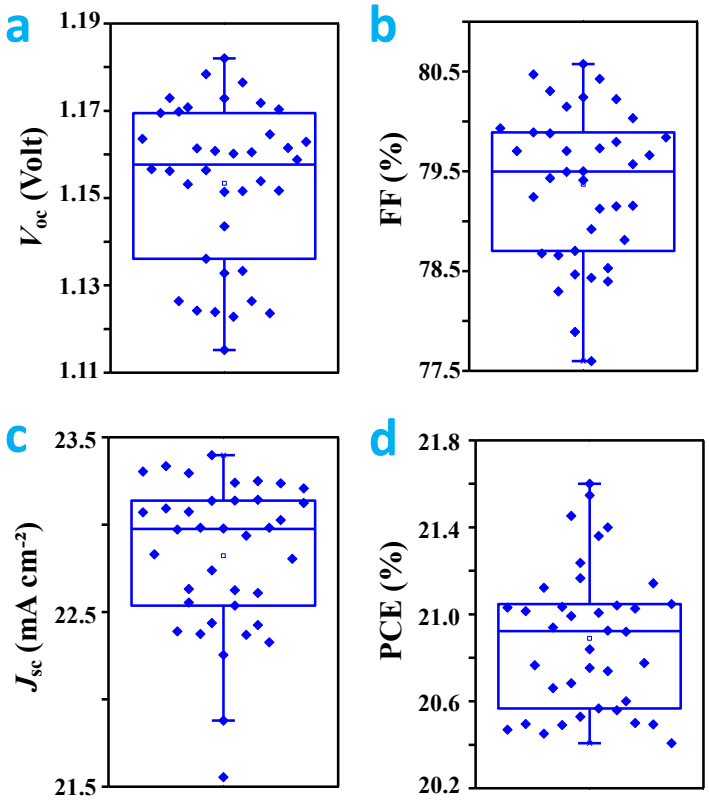

Figure S7. Statistic of photovoltaic parameters for optimal device TNG50 prepared from a different batch. (a) V_{oc}, (b) FF, (c) J_{sc} and (d) PCE of the PSC device.

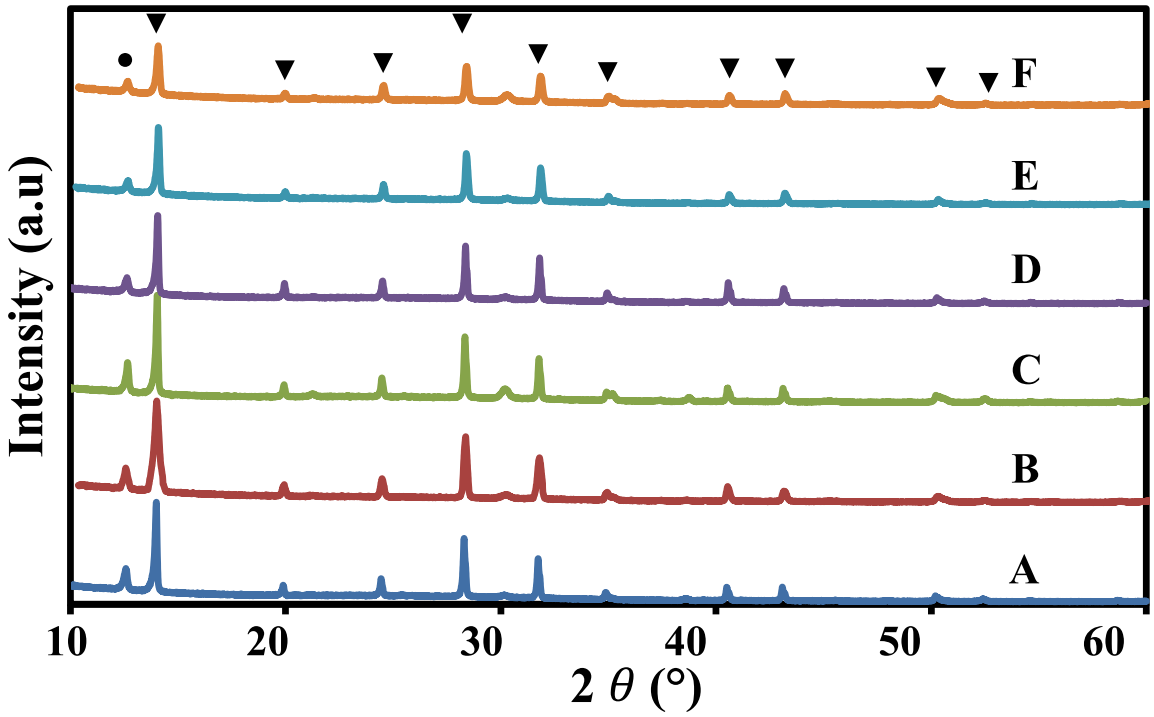

Figure S8. X-ray diffraction spectra of triple cation perovskite on TNG with different length. (A) TNG25 (40 nm), (B) TNG50 (80 nm), (C) TNG75 (120 nm), (D) TNG100 (250 nm), (E) TNG125 (200 nm) and (F) TNG150 (200) nm. (▼= $Cs_{0.05}[MA_{0.13}FA_{0.87}]_{0.95}Pb(I_{0.87}Br_{0.13})_3$, ● = PbI_2).

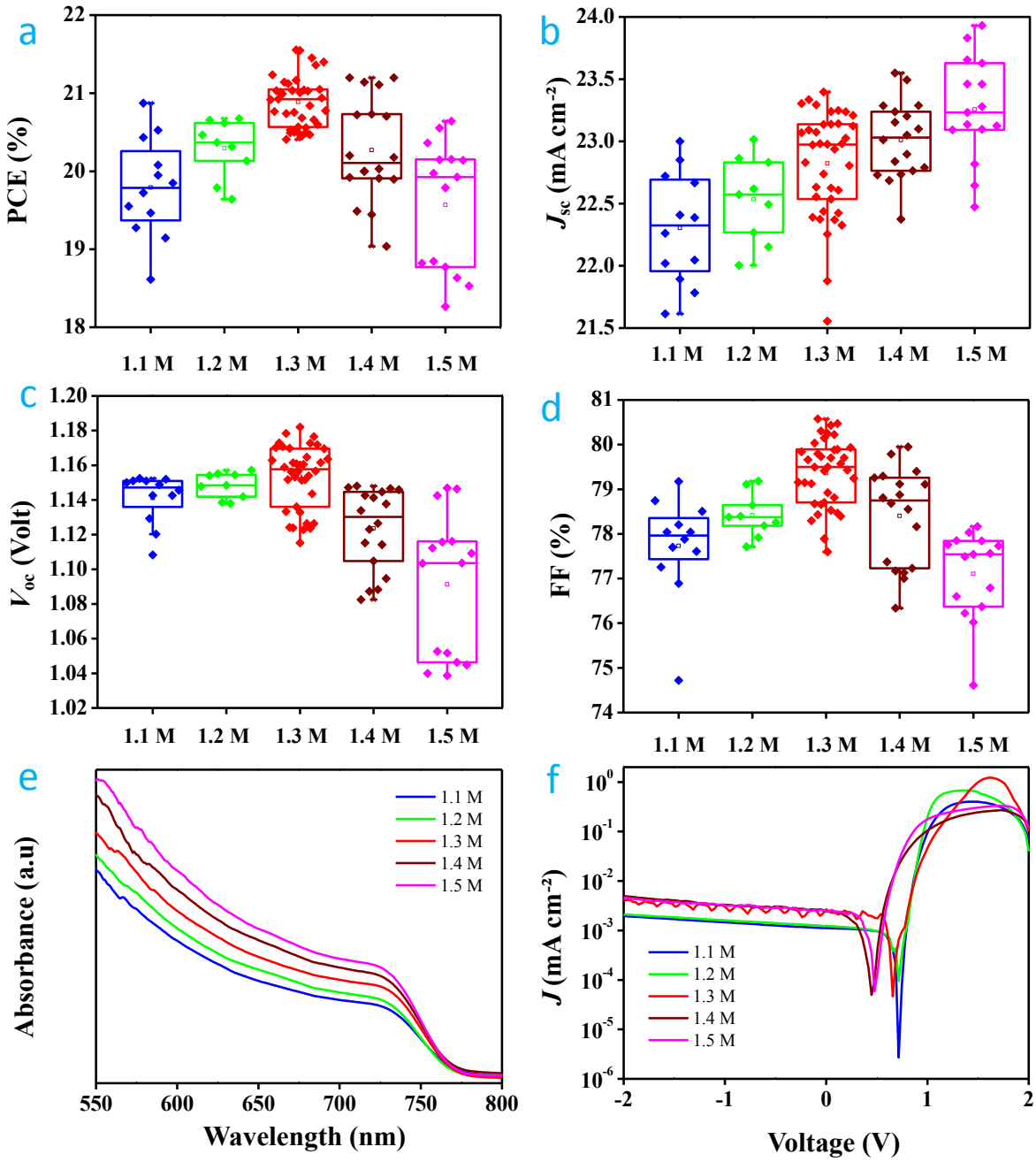

Figure S9. Photovoltaic performance of TNG-based PSC using different concentration of perovskite. (a to d) Statistic for PCE, J_{sc}, V_{oc} and FF. (e) perovskite absorbance and (f) devices dark-current profile.

Method for calculating the power hysteresis index (*HI*).

The power hysteresis of the device is calculated using the relation:

$$HI=(J_R^{(0.8Voc)}-J_F^{(0.8Voc)})/J_R^{(0.8Voc)}, \qquad \text{(eq. 1)}$$

where HI, $J_R^{(0.8Voc)}$ and $J_F^{(0.8Voc)}$ are hysteresis index and reverse and forward scans current density at voltage at $0.8V_{oc}$, respectively. For the case of SnO_2 based PSC, the $J_R^{(0.8Voc)}$ and

$J_F^{(0.8Voc)}$ obtained from the device are 19.864 and 17.398 mA cm^{-2}, respectively. By substituting the values into the eq. 1, the *HI* becomes:

HI=(19.864 - 17.398)/19.864

HI=0.12 or 12%.

Using similar way, the *HI* for the champion TNG based PSC device (TNG50) was found to be 0.10 or 10% as the $J_R^{(0.8Voc)}$ and $J_F^{(0.8Voc)}$ are 22.759 and 20.444 mA cm^{-2}, respectively. The *HI* for other devices is returned in Table S1.

Methods for calculating electron mobility

The electron mobility in the PSC device was predicted by fabricating an electron only device with structure of ITO/ETLs/Perovskite/PCBM/Au. The *J-V* response of the device was then recorded in the dark under nitrogen atmosphere. The double logarithmic plot of the result will contain a linear and a quadratic dependence of *J* over the applied bias *V* and a trap filling transition (TFL). The linear one is the Ohmic response of the device while the quadratic part is the space-charge limited current characteristic of the device, which is well-described using a Mott-Gurney relation[23] of: $J = \frac{9\varepsilon_r\varepsilon_0\mu_e V^2}{8L^3}$, where L, μ_e, ε_0 and ε_r are the thin film thickness (in this study, it is ca. 580 nm), electron mobility, vacuum permittivity and the relative dielectric constant of perovskite, respectively. The Moot-Gurney relation can be simplified as: $J = bV^2$ with $b = \frac{9\varepsilon_r\varepsilon_0\mu_e}{8L^3}$, which is obtained from second order polynomial fitting of the the quadratic part of the curve.

In our case, the perovskite dielectric constant and thickness are 46.9[24] and 580 nm, respectively. From the logarithmic *J-V* curve, we obtained the *b* value for TNG50, SnO_2 and planar TiO_2 based device are 3.242, 1.555 and 0.008, respectively, which yield electron mobility μ_e as high as 1.35×10^{-4}, 6.49×10^{-5} and 3.34×10^{-7} cm^2 V^{-1} s^{-1}, respectively.

References

1. B. Wang, J. Yang, L. Lu, W. Xiao, H. Wu, S. Xiong, J. Tang, C. Duan and Q. Bao, *Adv. Mater. Interfaces*, 2020, 1901964.
2. J. Chen, H. Dong, L. Zhang, J. Li, F. Jia, B. Jiao, J. Xu, X. Hou, J. Liu and Z. Wu, *J. Mater. Chem. A*, 2020, **8**, 2644-2653.

3. P. Zhu, S. Gu, X. Luo, Y. Gao, S. Li, J. Zhu and H. Tan, *Adv. Energ. Mater.*, 2020, **10**, 1903083.
4. T. Cao, K. Chen, Q. Chen, Y. Zhou, N. Chen and Y. Li, *ACS Appl. Mater. Interfaces*, 2019, **11**, 33825-33834.
5. X. Ren, D. Yang, Z. Yang, J. Feng, X. Zhu, J. Niu, Y. Liu, W. Zhao and S. F. Liu, *ACS Appl. Mater. Interfaces*, 2017, **9**, 2421-2429.
6. D. G. Lee, M.-c. Kim, B. J. Kim, D. H. Kim, S. M. Lee, M. Choi, S. Lee and H. S. Jung, *Appl. Surf. Sci.*, 2019, **477**, 131-136.
7. L. Hong, Y. Hu, A. Mei, Y. Sheng, P. Jiang, C. Tian, Y. Rong and H. Han, *Adv. Funct. Mater.*, 2017, **27**, 1703060.
8. Y. You, W. Tian, L. Min, F. Cao, K. Deng and L. Li, *Adv. Mater. Interfaces*, 2020, **7**, 1901406.
9. H. B. Lee, M. K. Jeon, N. Kumar, B. Tyagi and J. W. Kang, *Adv. Funct. Mater.*, 2019, **29**, 1903213.
10. T. Singh, S. Öz, A. Sasinska, R. Frohnhoven, S. Mathur and T. Miyasaka, *Adv. Funct. Mater.*, 2018, **28**, 1706287.
11. M. M. Tavakoli, P. Yadav, R. Tavakoli and J. Kong, *Adv. Energ. Mater.*, 2018, **8**, 1800794.
12. P. You, G. Li, G. Tang, J. Cao and F. Yan, *Energy Environ. Sci.*, In Press, DOI: 10.1039/C9EE02324K.
13. S. Li, P. Zhang, H. Chen, Y. Wang, D. Liu, J. Wu, H. Sarvari and Z. D. Chen, *J. Power Sources*, 2017, **342**, 990-997.
14. H. Yu, J. Roh, J. Yun and J. Jang, *J. Mater. Chem. A*, 2016, **4**, 7322-7329.
15. Y. W. Noh, J. H. Lee, I. S. Jin, S. H. Park and J. W. Jung, *Nano Energ.*, 2019, **65**, 104014.
16. A. J. Yun, J. Kim, T. Hwang and B. Park, *ACS Appl. Energ. Mater.*, 2019, **2**, 3554-3560.
17. J. Ren, Q. Luo, Q. Hou, H. Chen, T. Liu, H. He, J. Wang, Q. Shao, M. Dong and S. Wu, *ChemElectroChem*, 2019, **6**, 3167-3174.
18. S. You, H. Wang, S. Bi, J. Zhou, L. Qin, X. Qiu, Z. Zhao, Y. Xu, Y. Zhang and X. Shi, *Adv. Mater.*, 2018, **30**, 1706924.
19. M. Batmunkh, C. J. Shearer, M. Bat-Erdene, M. J. Biggs and J. G. Shapter, *ACS Appl. Mater. Interfaces*, 2017, **9**, 19945-19954.
20. Y. Shao, Y. Yuan and J. Huang, *Nat. Energ.*, 2016, **1**, 1-6.

21. Y. Bai, Q. Dong, Y. Shao, Y. Deng, Q. Wang, L. Shen, D. Wang, W. Wei and J. Huang, *Nat. Commun.*, 2016, **7**, 1-9.
22. M. Bag, L. A. Renna, R. Y. Adhikari, S. Karak, F. Liu, P. M. Lahti, T. P. Russell, M. T. Tuominen and D. Venkataraman, *J. Am. Chem. Soc.*, 2015, **137**, 13130-13137.
23. M. A. Lampert and P. Mark, *Current injection in solids*, Academic Press, New York, 1970.
24. R. Singh, S. Sandhu, H. Yadav and J.-J. Lee, *ACS Appl. Mater. Interfaces*, 2019, **11**, 29941-29949.